ACS OMEGA

http://pubs.acs.org/journal/acsodf

Article

Assessing the 3D Printability of an Elastomeric Poly(caprolactone-*co*-lactide) Copolymer as a Potential Material for 3D Printing Tracheal Scaffolds

Rahul V.G., Jijo Wilson, Lynda V. Thomas, and Prabha D. Nair*

Cite This: *ACS Omega* 2022, 7, 7002−7011

Read Online

ACCESS | Metrics & More | Article Recommendations

ABSTRACT: The advent of 3D printing technology has made remarkable progress in the field of tissue engineering. Yet, it has been challenging to reproduce the desired mechanical properties of certain tissues by 3D printing. This was majorly due to the lack of 3D printable materials possessing mechanical properties similar to the native tissue. In this study, we have synthesized four different ratios of poly(caprolactone-*co*-lactide (PLCL) and tested their 3D printing capabilities. The physicochemical properties of the material were characterized using Fourier-transform infrared (FTIR) spectroscopy, nuclear magnetic resonance (NMR) spectroscopy, gel permeation chromatography (GPC), and differential scanning calorimetry (DSC). Furthermore, the mechanical properties were assessed using the universal testing machine (UTM). The ratio with the higher lactide content was found to have better printability. Out of the different ratios assessed, a suitable ratio having the desired mechanical properties and printability was identified and 3D printed into a tracheal scaffold. Thus, PLCL can be a potential material for 3D printing of tissues like the trachea.

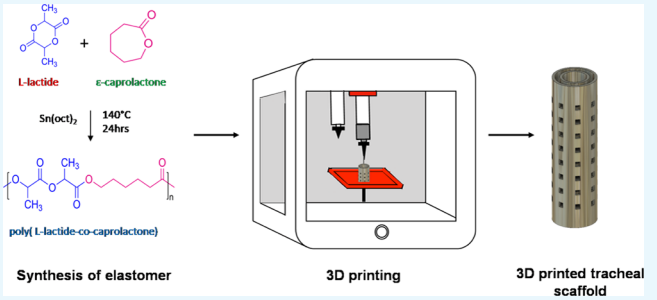

INTRODUCTION

Disorders and damages affecting the trachea often result in tracheal stenosis. In such cases, the damaged part is surgically removed and the remaining ends are joined by end-to-end anastomosis. However, if the defective region is more than 6 cm long, this procedure is not possible. It can be applied only in conditions where the damaged part is less than 50% of the length of the total trachea.[1] Although defects more than 6 cm are being treated now by stenting, it does not provide a permanent cure. Hence, there were attempts to find a tissue substitute to replace the defective tissue.[2] Autologous tissues like the aorta and esophagus, which are expected to have low immune reaction and better tissue integration, were used as a tracheal substitute. However, these candidates were mechanically inferior to the native tracheal cartilage and failed to provide the required mechanical strength for the trachea.[3−5]

In recent years, the focus has been on tissue engineered tracheal grafts that have comparable mechanical properties as those of the native trachea. For decades, several fabrication methods have been used to make the cylindrical constructs. Among them, electrospinning is the most widely used technique because of its easiness to make cylindrical scaffolds with nano fibrous morphology. However, it is difficult to fabricate the cartilage ring structures by this method, and hence, such scaffolds lack the mechanical stability that is imparted by the ring structures. With the advent of 3D printing technology, scaffolds for tracheal tissue regeneration having the desired shape and features are being fabricated with precision and accuracy.[6] Depending on the tissue, different materials are being used for 3D printing[7,8] Since the trachea is flexible, 3D printing using rigid materials may cause mechanical mismatch and subsequent graft failure. Polymeric materials having elastic properties and printability are ideal for 3D printing tracheal constructs.[9]

PLA (polylactic acid), PCL (polycaprolactone), and PGA (polyglycolic acid) are some of the commonly used FDA-approved implant materials. PLA and PCL are widely being used for 3D printing applications.[10−12] There are many studies showing the 3D printing capabilities of both the materials, which have been used for the fabrication of 3D printed trachea and its in vivo implantation.[6,13,14] While PLA is brittle, PCL is an elastic polymer with excellent load bearing properties.[15] PLA can be considered as an ideal material for 3D printing intricate structures because of its bridging capability, precision, and easy extrudability. However, it is very brittle and the

Received: November 25, 2021
Accepted: January 24, 2022
Published: February 20, 2022

https://doi.org/10.1021/acsomega.1c06679
ACS Omega 2022, 7, 7002−7011

printed structure is not preferred for load bearing applications.[16] Meanwhile, PCL is an elastomeric polymer and has attractive mechanical properties, but compared to PLA, PCL has limitations in printing intricate structures.[17] Even though there are many studies where PCL has been used for the fabrication of 3D printed trachea, compared to the native tissue, the material is stiff and lacks flexibility.[18] Hence, a material having 3D printability and elastomeric nature is highly desirable for 3D printing tracheal scaffolds. A copolymer of L-lactide (LA) and caprolactone (CL) is expected to have the crystallinity of the lactide and elasticity of the caprolactone, and its mechanical properties can be tuned by changing its monomeric ratio. Here, four different ratios of the copolymer were synthesized by ring opening polymerization, and the ratio having the suitable mechanical property and 3D printability was identified.[19]

RESULTS

Synthesis and Characterization of Poly(caprolactone-*co*-lactide). The PLCL copolymers were synthesized by ring opening polymerization at 140 °C [19] (Figure 1). Copolymers

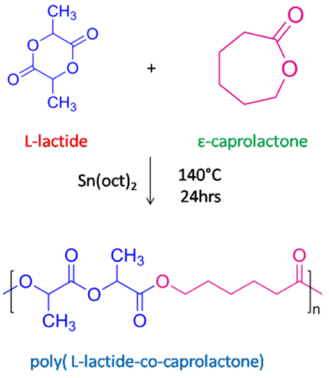

Figure 1. Synthesis of poly(caprolactone-*co*-lactide) by ring opening polymerization.

were synthesized in four different ratios of caprolactone and lactide. The feed monomer ratios of lactide and caprolactone were 65:35, 70:30, 80:20, and 90:10. The reaction was performed in a nitrogen atmosphere using stannous octoate as the catalyst for 24 h. Previous studies have shown that the highest molecular weight and yield were obtained at 140 °C using a comonomer/catalyst ratio of 2000:1.[20] It has also been reported that with the increase in the time of reaction, the lactide content changes.[19] Hence, a change in material property is also expected. Since the desired mechanical property was achieved at the above reported conditions, we performed the synthesis as per the protocol set by Garkhal et al. (2007).

FTIR Characterization of Poly(caprolactone-*co*-lactide). The FTIR spectra of the different carbon compounds present in the synthesized copolymer were analyzed at different wavelengths. The peak at 1750 cm^{-1} corresponds to the carbonyl stretching of lactide and caprolactone. The bands present in the 1000−1300 cm^{-1} region correspond to the ester group present, and the band at 1184 cm^{-1} is attributed by the long alkyl chain ester present in the polymer. The peaks at 2990 and 2945 cm^{-1} are attributed to the alkyl groups of lactide, and the peak at 2860 cm^{-1} is attributed to the alkyl group of caprolactone. The peak at 750 cm^{-1} corresponds to the characteristic methylene group of caprolactone, which became more prominent with an increase in the caprolactone ratio (Figure 2).

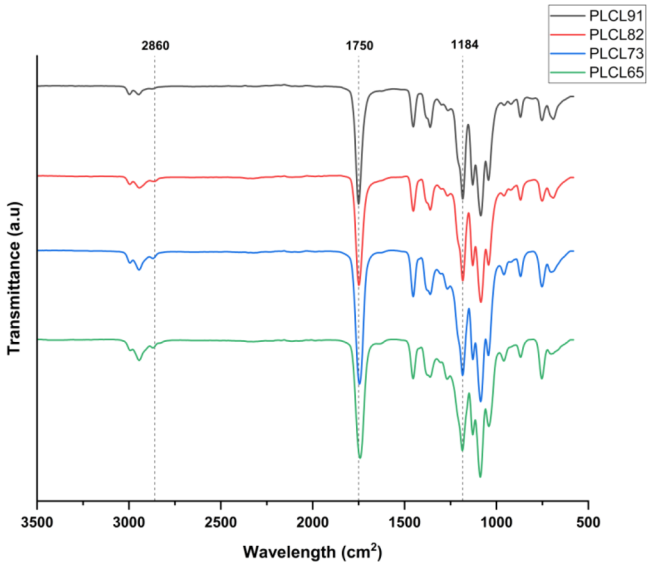

Figure 2. FTIR spectrum of four ratios of the synthesized PLCL copolymer.

Chemical Structure of the Synthesized Poly(caprolactone-*co*-lactide) Confirmed by NMR. The structure of the synthesized copolymer was confirmed by proton nuclear magnetic resonance spectra (Figure 3). The spectrum of PLCL showed peaks at 1.57 and 5.1 ppm that correspond to the CH_3 and CH moieties of lactide. The signal at 1.35−1.67 ppm corresponds to the alkyl groups of caprolactone. The signals around 2.3 and 4.03 ppm correspond to the α and ε methylene of the caprolactone. The signals at 2.4, 4.1, and 5.0 ppm confirmed the presence of CL−LA linkage and were present in all the ratios. The peaks of lactide protons were prominent in the PLCL91 spectrum. With the increase in the caprolactone ratio, the caprolactone peaks started appearing at 2.3 and 4.03 ppm. The molar ratios of CL/LA present in the PLCL copolymers were calculated by the integrated intensity ratio of the peak at 5.1 ppm for the LA unit and 4.1 ppm for the CA unit and were found to be similar to the feed molar ratio (Table 1).

Differential Scanning Calorimetry Showed That the Synthesized Copolymers Are Random Copolymers. The melting points of all the ratios of the synthesized PLCL were in between the melting points of PLA and PCL as shown in Figure 4. Since all the synthesized copolymers have single melting peaks, it confirms that the copolymer formed is a random copolymer. The ratios PLCL91 and PLCL82 have a Tg value of 46 °C, whereas the ratios PLCL73 and PLCL65 have a Tg value of 18 °C. Since the ratios with less lactide content have Tg values less than the room temperature, they exist in their amorphous state with low crystallinity, which indicates that the ratios are elastomeric in nature. This may be attributed to the increase in the methylene groups between the ester moieties with the increase in the caprolactone monomer in the feed ratios, which imparts more chain flexibility. All the ratios showed a cold crystallization peak at around 80 °C. The cold crystallization is observed when the polymer is mainly in an amorphous yet crystallizable state. At Tg, the polymeric

https://doi.org/10.1021/acsomega.1c06679
ACS Omega 2022, 7, 7002−7011

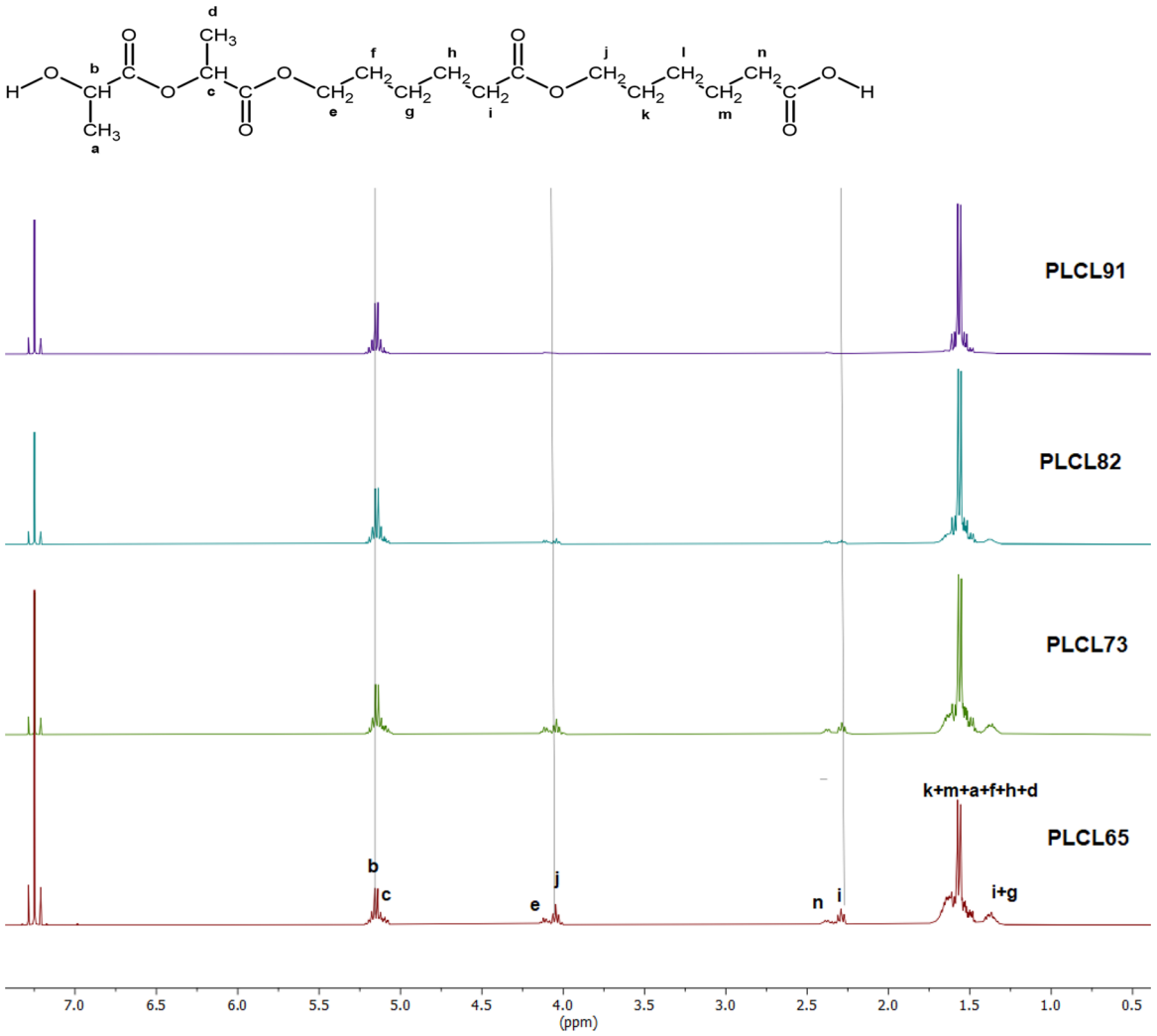

Figure 3. NMR spectroscopy based confirmation of the poly(caprolactone-*co*-lactide) structure. The characteristic peak shifts at 1.57 ppm (CH_3, LA), 5.1 ppm (CH, LA), 1.3−1.6 ppm ($CH_2CH_2CH_2$, CL), 2.3 ppm (CH_2 CO, CL), and 4.03 ppm (CH_2 O, CL) and the LA−CL junction at 2.4, 4.1, and 5 ppm.

Table 1. Summary of Physicochemical Properties of the PLCL Copolymer

	feed mol. ratio		copolymer composition							
sample	LA %	CL %	LA %	CL %	Tm (°C)	Tg (°C)	Xc (%)	tensile strength (MPa)	elongation at break (%)	MW
PLCL91	90	10	89	11	161	46	52.0	15.6 ± 2	5.15 ± 0.9	15,8329
PLCL82	80	20	76.1	23.9	150	46	51.3	18.7 ± 3	7.6 ± 0.2	96,022
PLCL73	70	30	67	33	133	18	39.2	63.4 ± 3	99.8 ± 2	80,835
PLCL65	65	35	47.8	52.2	128	18	20.4	112.5 ± 7	200.47 ± 9	34,335

chain attains a certain mobility; as the temperature is raised, the chains reorganize and form crystals, which result in the exothermic peak in the heating curve, and a further rise in the temperature causes the melting of the polymer. In the case of PLCL, the presence of caprolactone increases the chain mobility and results in the crystallization of the lactide content on melting. The percentage crystallinity was found to increase with the increase in the lactide content. There was a slight increase in the melting point with the lactide content, and the intensity of the melting peak was also found to be increasing with the increase in the lactide content.

Thermal Stability of PLCL Measured by TGA Analysis. Since FDM (fused deposition modeling) based 3D printing involves the melting of the polymer, the thermal stability of the synthesized polymer is an important factor to study. Figure 5 shows the TGA curves of four different ratios of the synthesized PLCL; with the increase in the caprolactone content, there is an evident increase in the degradation temperature (Table 2). Hence, the addition of caprolactone is found to increase the heat stability of the material.

Water Contact Angle of the PLCL Shows an Increase in Hydrophobicity with a Corresponding Increase in Lactide Content. Since there are more ester groups on the backbone of lactide than the caprolactone where the ester group is between five methyl groups on the backbone chain, the copolymers with more lactide groups are expected to be

https://doi.org/10.1021/acsomega.1c06679
ACS Omega 2022, 7, 7002−7011

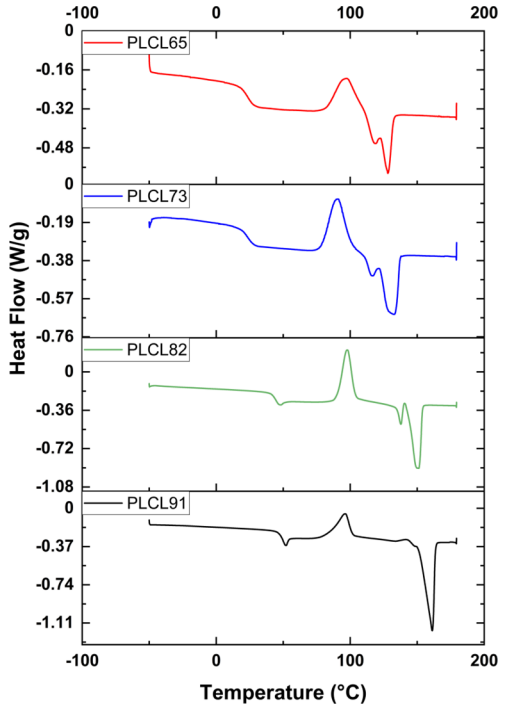

Figure 4. Differential scanning calorimetry of the four different ratios of the synthesized PLCL.

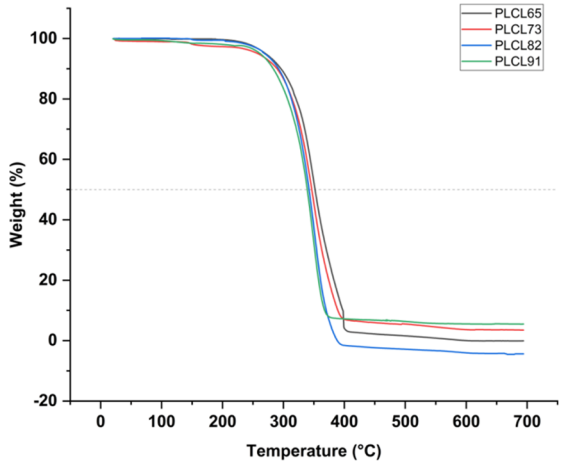

Figure 5. Thermogravimetric analysis (TGA) of four ratios of PLCL synthesized.

Table 2. Degradation Temperature of PLCL

sample	Td (°C)
PLCL91	339
PLCL82	346
PLCL73	342
PLCL65	351

more hydrophilic than the copolymers of lower lactide ratios. This is confirmed by the water contact angle measurement of the copolymer films where the copolymer PLCL65 showed a hydrophobic water contact angle of 98.1°, PLCL73 showed a contact angle of 89.1°, PLCL82 showed a contact angle of 78.3°, and PLCL91 showed a contact angle of 75.6° (Figure 6).

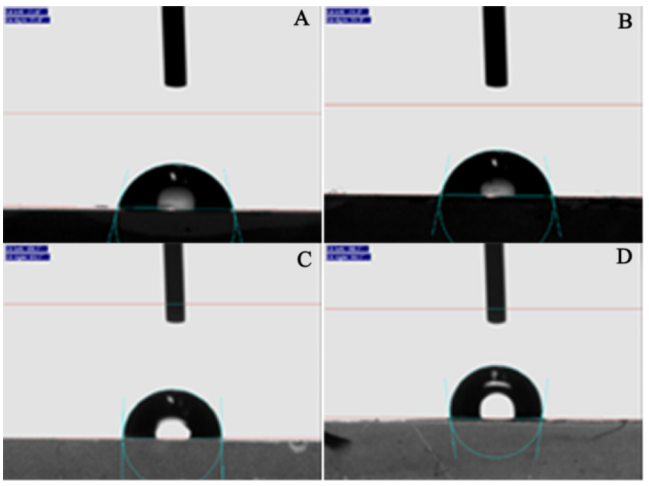

Figure 6. Water contact angle showing the hydrophilicity of the synthesized copolymer (A) PLCL91, (B) PLCL82, (C) PLCL73, and (D) PLCL65.

Mechanical Testing of PLCL by UTM. The mechanical properties of the material change with the copolymerization reaction using different monomer feed ratios. To probe the material properties in terms of stiffness and elasticity ideally required for tracheal tissues, mechanical testing of the synthesized polymers was performed and evaluated. Rectangular films of 0.02 mm thickness made by solvent casting were stretched apart in the UTM, and the stress strain graph was plotted. Figure 7 shows the stress−strain curve of the different

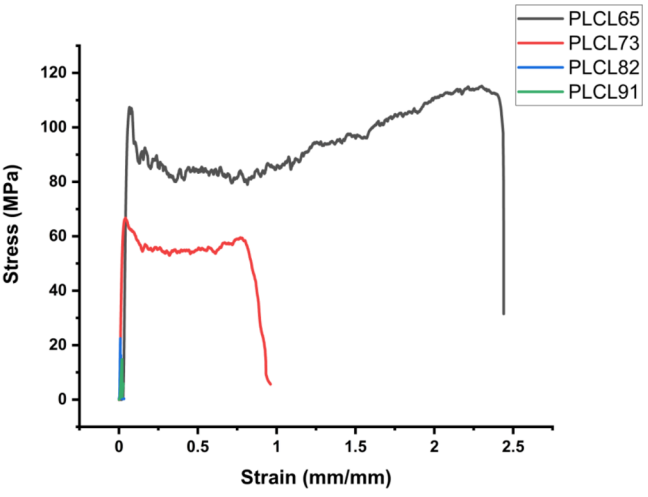

Figure 7. Stress−strain curve of the synthesized PLCL.

ratios of the synthesized PLCL. The higher ratios PLCL91 and PLCL82 represent a typical glassy behavior with immediate failure after the yield point with higher crystallinity as evidenced from the DSC thermograms, whereas PLCL65 and PLCL73, due to their increased caprolactone content, showed an elastic behavior with an elongation at break of 200.47 ± 9 and 99.8 ± 2% and tensile strength of 63.4 ± 3 and 112.5 ± 7, respectively, showing that the synthesized material is mechanically superior to the native rabbit trachea.[21] Since the higher ratios were brittle and less elastic, PLCL65 and PLCL73 were chosen for our further 3D printing studies.

Cytotoxicity of the Material Tested by Live Dead Staining. Live/dead staining was used to evaluate the viability

https://doi.org/10.1021/acsomega.1c06679
ACS Omega 2022, 7, 7002−7011

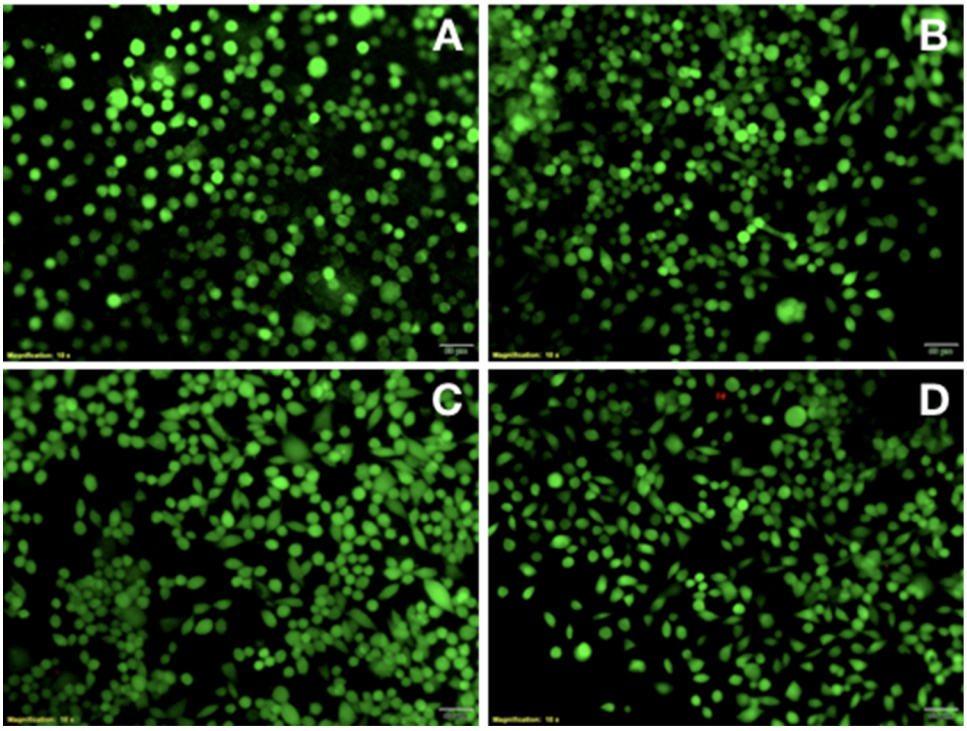

Figure 8. Live/dead staining of L929 cells cultured on the different ratios of PLCL: (A) PLCL65, (B) PLCL73, (C) PLCL82, and (D) PLCL91.

of the cells seeded on the PLCL. The live cells stained with calcein showed green fluorescence, and the dead cells stained with EtBr showed red fluorescence. In Figure 8, the cells have a round shape in the PLCL65 ratio, which has a higher caprolactone content. There were negligible or no cells with a fibroblastic morphology seen due to the higher hydrophobicity of the PLCL65 ratio, whereas the number of cells with fibroblastic morphology was found to be increasing with the increase in the lactide content. In PLCL73 few cells with the fibroblastic morphology were observed. However, in PLCL82 and PLCL91 more cells with fibroblastic morphology can be seen, which is due to the increase in the hydrophilicity of the material. All the ratios showed little or negligible dead cells after 2 days of the culture.

Cell Proliferation Analysis by MTT Assay. The proliferation of L929 cells on all the ratios of the PLCL material extract was evaluated by the MTT assay. Figure 9 shows that all the four ratios of the PLCL showed comparable cell proliferation as that of the tissue culture plate in the MTT assay of 1, 7, and 14 days of extract. The percentage cell viability of PLCL91, PLCL82, PLCL73, and PLCL65 on the extract of day 1 was 93 ± 7, 97 ± 4, 93 ± 3, and 92 ± .5%, respectively, and that of 7 days was 89 ± 5, 94 ± 4, 90 ± 3, and 84 ± 3%. The 14 day extract showed 90.3 ± 2, 92 ± 3, 86 ± 4, and 85.8 ± 2% cell viability, respectively. Even though there was a difference in the percentage cell viability between different ratios of PLCL and the tissue culture plate, it was not significant ($p > 0.05$). Hence, the in vitro cytotoxic studies showed that all the ratios of PLCL do not have any cytotoxic effect up to 14 days of incubation and are capable of supporting the growth of the cells.

Standardization of 3D Printing Parameters of PLCL. The print speed, nozzle temperature, and pressure are the key factors that decide the precision and accuracy of the printed structure. These parameters have been standardized by using

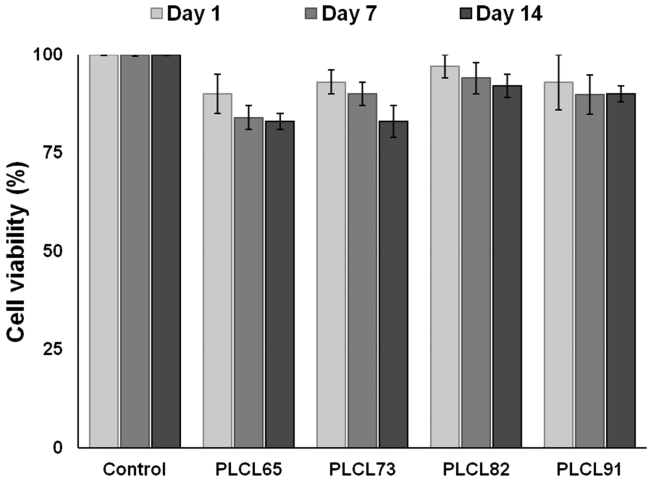

Figure 9. MTT assay of different ratios of PLCL and the tissue culture plate showing comparable cell proliferation.

previously reported methods.[22] The appropriate ratio for our application was identified based on these results. Since the higher ratios PLCL91 and PLCL82 were found to be brittle (Figure 7), we used elastomeric ratios PLCL73 and PLCL65 for the 3D printing studies. Both of these ratios were found to be elastomeric and suitable for our application.

The print speed, nozzle temperature, and pressure of PLCL65 and PLCL73 were identified by the line drawing method. Lines were drawn at different speeds, temperatures, and pressures, and the values at which the line produced similar width as that of the nozzle diameter were chosen for further 3D printing experiments. Figure 10A,B shows the standardization of speed of PLCL65 by the line drawing method; the lines were drawn at 6−10 mm/s. As the speed increased, the width of the line decreased. A speed of 9 mm/s produced a width of about 850 μm, which is the same as the

https://doi.org/10.1021/acsomega.1c06679
ACS Omega 2022, 7, 7002−7011

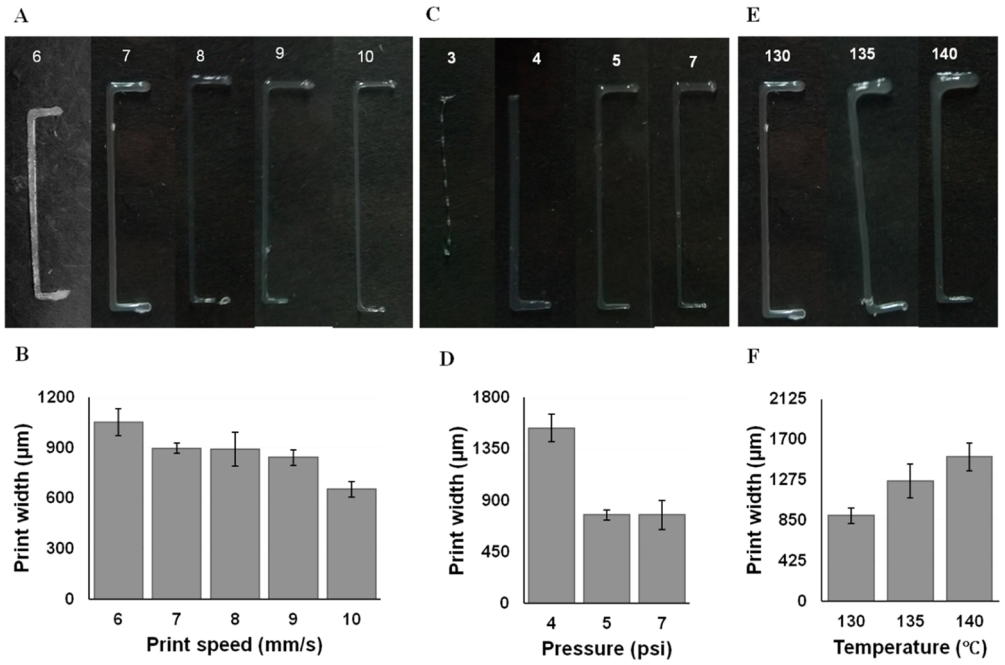

Figure 10. Standardization of printing parameters of PLCL65 by the line drawing method. (A, B) Speed, (C, D) pressure, and (E, F) temperature.

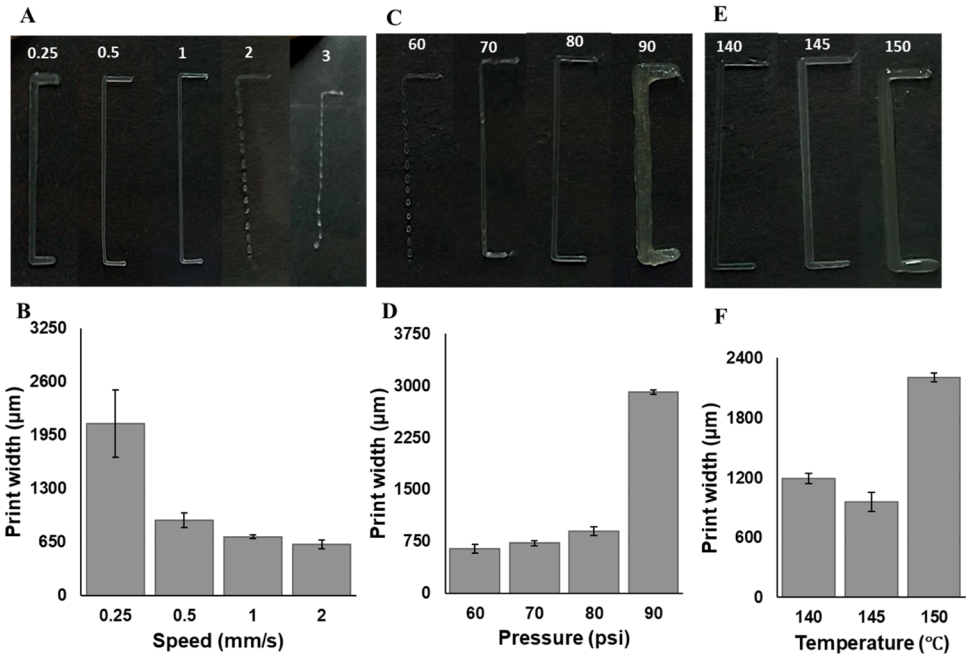

Figure 11. Standardization of printing parameters of PLCL73. (A, B) Speed, (C, D) pressure, and (E, F) temperature.

nozzle diameter. For pressure, a speed of 9 mm/s was used and the width increased with the increase in the pressure from 3 to 7 psi. At 3 psi, the extrusion was too slow and produced dotted lines; there was no extrusion at pressures below 3 psi. A pressure of 5 psi produced a line width of 850 mm (Figure 10C,D). The temperature was standardized at a speed of 9 mm/s and pressure of 5 psi. The line width increased in the range from 850 to 1300 μm with the increase in the temperature from 130 to 145 °C. A temperature of 130 °C produced a line width of 850 μm (Figure 10E,F). The printing parameters for the PLCL73 ratio were also standardized similarly, and the values of speed, pressure, and temperature were found to be 0.5 mm/s, 80 psi, and 140 °C, respectively (Figure 11). In the case of PLCL73, the molecular weight was high compared to PLCL65, which has increased the melt viscosity index of PLCL73. This was evident while extruding the polymer out of the nozzle. PLCL65 was extruding easily compared to PLCL73. Hence, the print pressure and print temperature required for the PLCL65 ratio were very low compared to the PLCL73 ratio. However, the print accuracy of PLCL73 was much better when compared to the PLCL65 ratio and was further subjected to printability testing to ascertain the print quality.

The printability of the materials was evaluated by using the grid method described in the previous studies. Even though this has been used only for the gel systems, since it involves the

https://doi.org/10.1021/acsomega.1c06679
ACS Omega 2022, 7, 7002−7011

transition of molten polymer from the liquid state to the solid state, the same method can be used for the evaluation of the polymers used in FDM printers as well. If the extruded polymer has a lower curing time and solidifies shortly after the extrusion, it will produce a print with constant dimensions. This improves the print precision and would produce regular grid structures with perfect squares. If the polymer still has flowability, the upper and lower layers would fuse and produce irregular grids or squares with round corners and form circle-like structures. The printability of the materials can be evaluated by how close the structure is to a perfect square; this is defined by eq 3.

Although PLCL65 is more elastic than PLCL73 when subjected to mechanical tensile pull, the material takes more time to cure after extrusion, which affects the printability of the material. This was evident from the higher printability value of 1.24 for PLCL65 (Figure 12A). Meanwhile, PLCL73 was found to have a printability of 1.012, which shows that the print quality was maintained as the Pr value of PLCL73 was close to 1, which was also evident in the almost perfect squares printed in the grid (Figure 12B).

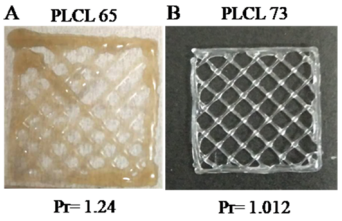

Figure 12. Printability evaluation of (A) PLCL65 and (B) PLCL73 by the grid method.

Filament Collapse Test. The shape fidelity and bridging capacity play a major role in 3D printing complex structures. The shape fidelity and bridging capacity of PLCL65 and PLCL73 were measured by printing the material over gaps of size 5, 10, 15, and 20 mm and measuring the area under the filament. Since PLCL65 is inferior to PLCL73 in terms of print fidelity, the printed filament started bending even from the 10 mm gap and failed to connect the 20 mm gap (Figure 13A). The presence of a higher lactide content improved the print fidelity of PLCL73; this was evident in Figure 13B. Compared to PLCL65, PLCL73 had more collapse area factor (C_f) (Figure 13C), and the material formed a stable bridge at the 20 mm gap. Even though PLCL65 was more elastic, it was lacking printability. The PLCL75 ratio was found to be elastic and showed good printability. Hence, the PLCL75 ratio was found to be the appropriate ratio for our 3D printing application.

3D Printing of PLCL73 into the Trachea. A tracheal scaffold having shape and dimensions similar to the native rabbit trachea was designed using the fusion360 software (Design registration no: 323114-001). The total length of the scaffold is 3.5 cm, and it has an inner diameter of 5 mm. The structure has two suturing rings of 2 mm length on both ends of the scaffold. Along the length, the structure has ″C″ shaped rings of 1 mm width, which are placed 2 mm apart, and there are connecting ribs of 1 mm width connecting the inner and outer cylinders. The present structure (Figure 14) is designed for the generation of a biphasic tracheal construct, where a hydrogel with cells can be used to fill the gap between the two cylinders. The cylindrical structure discussed in this study was printed using PLCL73 at 140 °C at a speed of 0.5 mm/s and pressure of 80 psi using a 20 gauge nozzle. Good printability and accuracy in shape features were obtained on printing with PLCL73, which proved that the PLCL with a monomer feed ratio of 7:3 was ideal for printing applications (Figure 15). Moreover, the elasticity and mechanical stability in addition to the cytocompatibility imparted by the polymer were much superior to the commonly used PCL ink on 3D printing and hence could find potential applications in 3D printing of tracheal constructs and other medical implants and constructs.

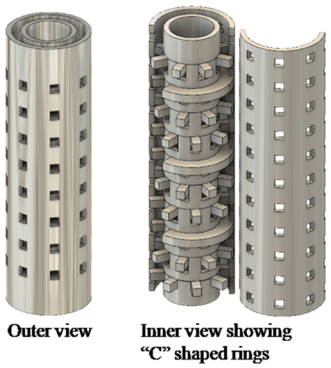

Figure 14. CAD-based design of the tracheal scaffold.

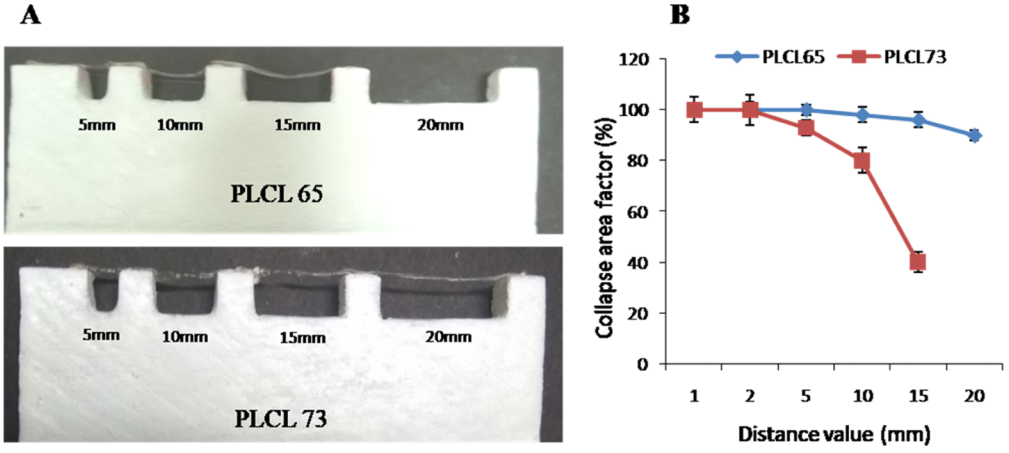

Figure 13. Filament collapse test of (A) PLCL65 and (B) PLCL73. (C) PLCL73 showing better stability than PLCL65.

https://doi.org/10.1021/acsomega.1c06679
ACS Omega 2022, 7, 7002−7011

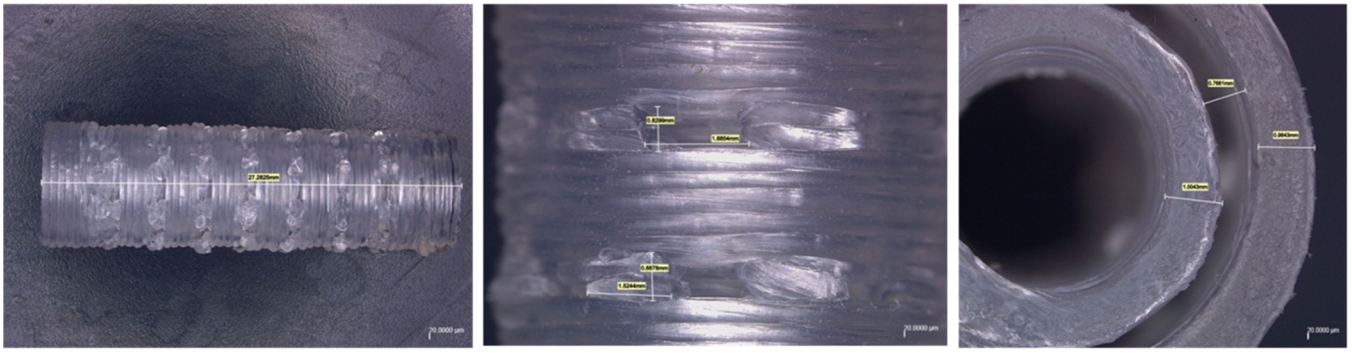

Figure 15. Images of the 3D printed PLCL tracheal scaffold of PLCL73.

DISCUSSION

Despite the advances in tissue engineering technologies, a clinically reliable tissue engineered trachea is yet to make a mark in translational medicine. Several recent attempts have been made towards repairing the tracheal defect using 3D printed tracheal constructs.[23] Most of these studies used biocompatible materials for 3D printing. However, their mechanical properties were not comparable with the native trachea.

The advent of 3D printing technology has opened various possibilities in the field of tissue engineering. Many of the grafts require personalized design and dimensions depending on the size and shape of the defect.[24] 3D printing helps to automate the whole process of tissue construction by printing the polymer along with the desired cells and growth factors into a predefined size and shape.[25] This work shows the potential of the PLCL copolymer, which has proven biocompatibility, desired mechanical properties, and degradation rate, to be used as a 3D printable material for printing intricate structures.[26]

Repairing long segmental tracheal defects is a challenging procedure for clinicians. Presently, it is done by transplanting donor organs. Apart from the difficulty in getting the donor, mechanical failure and inflammatory response are some of the major complications associated with the transplantation. In many cases, the grafts were later reinforced with a stent to allow them to remain open.[27]

In this study, we have designed an open structure having closely placed pores that will allow easy diffusion of nutrients and improve the vasculature throughout the graft. Since the material is elastomeric having comparable mechanical properties as those of the native trachea, the graft is expected to prevent complications associated with mechanical mismatch. There are many studies showing the biocompatibility of PLCL. Since it is a copolymer of caprolactone and lactide, they degrade to give non-toxic byproducts caproic acid and lactic acid, respectively, which are easily excreted from the body or resorbed through the metabolic pathways.[28]

The construct can be implanted orthotopically in a primary site like the peritoneal cavity or forearm. The construct is expected to integrate with the tissue and form the vasculature and fibrotic tissue. This implant can then be retrieved and grafted to the defective tracheal site, which might improve the chances of the graft survival.[2]

CONCLUSIONS

We have explored the potential of poly(lactide-*co*-caprolactone) as a 3D printable biomaterial and found that the synthesized PLCL73 ratio has the desired mechanical properties required for a tracheal scaffold. We were successful in designing and 3D printing an open structure tracheal scaffold using the aforementioned PLCL ratio. The material and the design need to be evaluated as a scaffold for tracheal replacement therapy. This is an initial study to evaluate the ideal copolymer system for 3D printing of tracheal tissue, and further in vivo studies to prove the efficacy and safety of the construct need to be performed.

METHODS

Synthesis of Poly(caprolactone-*co*-lactide). The ring opening polymerization technique was used for the synthesis of the PLCL polymer. Predetermined amounts of L-lactide and caprolactone were added to a clean round-bottom flask. The flask was purged with nitrogen for 30 min. Stannous octoate was added at a comonomer/catalyst ratio of 2000:1. The reaction was performed at 140 °C for 24 h. The product was dissolved in chloroform and precipitated in excess methanol to remove the unreacted reactants. The product was then dried at 45 °C.

FTIR Analysis. FT-IR spectra were recorded using a Bruker (ALPHA II) instrument in ATR mode having a zinc selenide crystal. The dried samples in pellet form were used, and a total of 25 scans were taken to acquire the spectrum. The infrared spectrum of the individual samples was recorded in the spectral range of 3500 to 500 cm^{-1} at 4 cm^{-1} resolution.

Analysis of Thermal Properties. TGA was performed using a TGA analyzer (TA Instruments, SDT 2920). The samples were heated up to 700 °C at a heating rate of 10 °C/min. The temperature at which 50% of the sample degraded was taken as the degradation temperature (Td). DSC analysis was performed using a Perkin Elmer DSC instrument calibrated with indium standards. Samples (5−10 mg) were cooled at −60 °C and heated to 250 °C at a heating rate of 10 °C/min under a nitrogen atmosphere. The percentage crystallinity was calculated using the following formula:

$$X_c\% = \frac{\Delta H_{m1} + \Delta H_{m2} - \Delta H_c}{\Delta H_m^0} \times 100 \quad (1)$$

where X_c is the degree of crystallization, ΔH_{m1} is the enthalpy of melting, ΔH_m^0 is the enthalpy of melting of the pure material, and ΔH_c is the enthalpy of crystallization and where ΔH_m^0 is 106 (J g^{-1} of PLLA).

Proton Nuclear Magnetic Resonance Spectroscopy. The H^1 NMR spectra of the samples were recorded using the Bruker instrument at 300 MHz of nuclear frequency. Samples

https://doi.org/10.1021/acsomega.1c06679
ACS Omega 2022, 7, 7002−7011

(5−10 mg) were solubilized in $CDCl_3$. The molar ratio of the copolymer was calculated by using the following formula:

$$\text{Mole \% of caprolactone} = \frac{\text{relative moles of caprolactone}}{\text{relative moles of caprolactone} + \text{relative moles of lactide}} \times 100 \quad (2)$$

Mechanical Testing. Mechanical testing of the samples was done using an Instron UTM (Universal Testing Machine) at room temperature. For performing this experiment, all four ratios of the synthesized PLCL were dissolved in chloroform and solvent casted into film strips of 12 mm width, 60 mm length, and 0.02 mm thickness. The samples were loaded on the instrument, and the experiment was conducted at a crosshead speed of 5 mm/min using a load cell of 10 N.

Live/Dead Staining. L929 fibroblast cells were trypsinized, seeded onto the PLCL scaffold, and incubated for 1.5 h to enable cell attachment, and then DMEM with 10% FBS media was added and cultured for 2 days. After 2 days, the scaffold was retrieved, washed in PBS, and stained with the calcein/EtBr (ethidium bromide, Thermofisher) stain prepared in PBS as per the manufacturer's protocol. After the staining, the samples were washed in PBS and fluorescence was observed under a fluorescence microscope (Olympus).

MTT Assay. The material in 1 mL of media was incubated at 37 °C for 1, 7, and 14 days, and the extract was collected and treated with L929 cells for 24 h. The media were removed, and the MTT solution prepared in PBS was added to the samples and incubated for 3 h. DMSO was added and mixed well to solubilize the formazan crystal. The absorbance was measured at 590 nm, and MTT prepared in PBS and DMSO was taken as the blank.

Scaffold Design and 3D Printing. The scaffold was designed using the fusion360 software. The design was similar to a native rabbit trachea, having 5 mm internal diameter and 3.5 cm length. The printing was done using a 20 gauge nozzle at a temperature of 140 °C, pressure of 80 psi, and speed of 0.5 mm/s. The dimensions of the structures were measured using a stereomicroscope and the ImageJ software. The evaluation of printability, standardization of printing parameters, and print fidelity were done as per the previously reported methods.[29] The printability was calculated using the following equation:

$$C = \frac{4\pi A}{L^2} \quad (3)$$

$$\text{Pr} = \frac{\pi}{4} \times \frac{1}{C} = \frac{L^2}{16A} \quad (4)$$

where Pr is the printability, C is the circularity, L is the perimeter of the square, and A is the area of the square.

The collapse area factor (C_f), which is the percentage of the area under the filament with respect to the theoretical area, was calculated using the following equation:

$$C_f = \frac{A_a^c}{A_t^c} \times 100$$

where A_a^c is the calculated area under the filament and A_t^c is the theoretical area between the pillars (Figure 13A).

Statistical Analysis. The data are expressed as mean ± standard deviation. The statistical comparison between the groups was done by one-way ANOVA followed by the Kruskal−Wallis post hoc test.

AUTHOR INFORMATION

Corresponding Author

Prabha D. Nair − *Division of Tissue Engineering and Regenerative Technologies, Biomedical Technology Wing, Sree Chitra Tirunal Institute for Medical Sciences and Technology, Thiruvananthapuram 695012 Kerala, India*; Email: vdnair70@gmail.com

Authors

Rahul V.G. − *Division of Tissue Engineering and Regenerative Technologies, Biomedical Technology Wing, Sree Chitra Tirunal Institute for Medical Sciences and Technology, Thiruvananthapuram 695012 Kerala, India*; orcid.org/0000-0002-5577-990X

Jijo Wilson − *Division of Tissue Engineering and Regenerative Technologies, Biomedical Technology Wing, Sree Chitra Tirunal Institute for Medical Sciences and Technology, Thiruvananthapuram 695012 Kerala, India*

Lynda V. Thomas − *Division of Tissue Engineering and Regenerative Technologies, Biomedical Technology Wing, Sree Chitra Tirunal Institute for Medical Sciences and Technology, Thiruvananthapuram 695012 Kerala, India*

Complete contact information is available at: https://pubs.acs.org/10.1021/acsomega.1c06679

Notes

The authors declare no competing financial interest.

ACKNOWLEDGMENTS

This study was supported by an Indo-Danish Grant from DBT India (BT/IN/DENMARK/08/JD/2016) and an SCTIMST institute fellowship. The authors thank the Director, SCTIMST, and Head, BMT wing, SCTIMST, for providing the facilities to carry out this work; Mr. Willi Paul for the DSC measurements; and Dr. Radhakumary C. for TGA measurements.

REFERENCES

(1) Ścierski, W.; Lisowska, G.; Namysłowski, G.; Misiołek, M.; Pilch, J.; Menaszek, E.; Gawlik, R.; Błażewicz, M. Reconstruction of Ovine Trachea with a Biomimetic Composite Biomaterial. *BioMed Res. Int.* **2018**, *2018*, No. e2610637.

(2) Delaere, P.; Van Raemdonck, D. Tracheal Replacement. *J. Thorac. Dis.* **2016**, *8*, S186−S196.

(3) Kato, R.; Eguchi, K.; Izumi, Y.; Kakizaki, T.; Hangai, N.; Sawafuji, M.; Yamamoto, T.; Kawamura, M.; Kikuchi, K.; Kobayashi, K. Experimental Tracheal Replacement Using the Esophagus and an Expandable Metallic Stent. *Surg. Today* **1995**, *25*, 806−810.

(4) Friedman, M.; Mayer, A. D. Laryngotracheal Reconstruction in Adults with the Sternocleidomastoid Myoperiosteal Flap. *Ann. Otol. Rhinol. Laryngol.* **1992**, *101*, 897−908.

(5) Propst, E. J.; Prager, J. D.; Meinzen-Derr, J.; Clark, S. L.; Cotton, R. T.; Rutter, M. J. Pediatric Tracheal Reconstruction Using Cadaveric Homograft. *Arch. Otolaryngol. Head Neck Surg.* **2011**, *137*, 583−590.

(6) Gao, M.; Zhang, H.; Dong, W.; Bai, J.; Botao, G.; Dekai, X.; Feng, B.; Chen, M.; He, X.; Yin, M.; Xu, Z.; Witman, N.; Fu, W.; Zheng, J. Tissue-Engineered Trachea from a 3D-Printed Scaffold Enhances Whole-Segment Tracheal Repair. *Sci. Rep.* **2017**, *7*, 1−12.

(7) Sing, S. L.; Wang, S.; Agarwala, S.; Wiria, F. E.; Ha, T. M. H.; Yeong, W. Y. Fabrication of Titanium Based Biphasic Scaffold Using Selective Laser Melting and Collagen Immersion. *Int. J. Bioprinting* **2017**, *3*, 007.

(8) Mustapha, K. B.; Metwalli, K. M. A Review of Fused Deposition Modelling for 3D Printing of Smart Polymeric Materials and Composites. *Eur. Polym. J.* **2021**, *156*, 110591.
(9) Jung, S.; Lee, S. J.; Kim, H.; Park, H.; Wang, Z.; Kim, H.; Yoo, J.; Chung, S.; Kim, H. S. 3D Printed Polyurethane Prosthesis for Partial Tracheal Reconstruction: A Pilot Animal Study. *Biofabrication* **2016**, *8*, No. 045015.
(10) Arora, J. K.; Bhati, P. Fabrication and Characterization of 3D Printed PLA Scaffolds. *AIP Conf. Proc.* **2020**, *2205*, No. 020065.
(11) Li, J.; Chen, M.; Wei, X.; Hao, Y.; Wang, J. Evaluation of 3D-Printed Polycaprolactone Scaffolds Coated with Freeze-Dried Platelet-Rich Plasma for Bone Regeneration. *Materials* **2017**, *10*, 831.
(12) Moncal, K. K.; Heo, D. N.; Godzik, K. P.; Sosnoski, D. M.; Mrowczynski, O. D.; Rizk, E.; Ozbolat, V.; Tucker, S. M.; Gerhard, E. M.; Dey, M.; Lewis, G. S.; Yang, J.; Ozbolat, I. T. 3D Printing of Poly(ε-Caprolactone)/Poly(D,L-Lactide-Co-Glycolide)/Hydroxyapatite Composite Constructs for Bone Tissue Engineering. *J. Mater. Res.* **2018**, *33*, 1972−1986.
(13) Park, S. A.; Lee, H.-J.; Kim, K.-S.; Lee, S. J.; Lee, J.-T.; Kim, S.-Y.; Chang, N.-H.; Park, S.-Y. In Vivo Evaluation of 3D-Printed Polycaprolactone Scaffold Implantation Combined with β-TCP Powder for Alveolar Bone Augmentation in a Beagle Defect Model. *Materials* **2018**, *11*, 238.
(14) Maia-Pinto, M. O. C.; Brochado, A. C. B.; Teixeira, B. N.; Sartoretto, S. C.; Uzeda, M. J.; Alves, A. T. N. N.; Alves, G. G.; Calasans-Maia, M. D.; Thiré, R. M. S. M. Biomimetic Mineralization on 3D Printed PLA Scaffolds: On the Response of Human Primary Osteoblasts Spheroids and In Vivo Implantation. *Polymer* **2021**, *13*, 74.
(15) Bruyas, A.; Lou, F.; Stahl, A. M.; Gardner, M.; Maloney, W.; Goodman, S.; Yang, Y. P. Systematic Characterization of 3D-Printed PCL/β-TCP Scaffolds for Biomedical Devices and Bone Tissue Engineering: Influence of Composition and Porosity. *J. Mater. Res.* **2018**, *33*, 1948−1959.
(16) Donate, R.; Monzón, M.; Alemán-Domínguez, M. E. Additive Manufacturing of PLA-Based Scaffolds Intended for Bone Regeneration and Strategies to Improve Their Biological Properties. *e-Polym.* **2020**, *20*, 571−599.
(17) Sodupe Ortega, E.; Sanz-Garcia, A.; Pernia-Espinoza, A.; Escobedo-Lucea, C. Efficient Fabrication of Polycaprolactone Scaffolds for Printing Hybrid Tissue-Engineered Constructs. *Materials* **2019**, *12*, 613.
(18) She, Y.; Fan, Z.; Wang, L.; Li, Y.; Sun, W.; Tang, H.; Zhang, L.; Wu, L.; Zheng, H.; Chen, C. 3D Printed Biomimetic PCL Scaffold as Framework Interspersed With Collagen for Long Segment Tracheal Replacement. *Front. Cell Dev. Biol.* **2021**, *9*, 33.
(19) Zhang, M.; Chang, Z.; Wang, X.; Li, Q. Synthesis of Poly(l-Lactide-Co-ε-Caprolactone) Copolymer: Structure, Toughness, and Elasticity. *Polymer* **2021**, *13*, 1270.
(20) Garkhal, K.; Verma, S.; Jonnalagadda, S.; Kumar, N. Fast Degradable Poly(L-Lactide-Co-ε-Caprolactone) Microspheres for Tissue Engineering: Synthesis, Characterization, and Degradation Behavior. *J. Polym. Sci. Part Polym. Chem.* **2007**, *45*, 2755−2764.
(21) Martínez-Hernández, N. J.; Mas-Estellés, J.; Milián-Medina, L.; Martínez-Ramos, C.; Cerón-Navarro, J.; Galbis-Caravajal, J.; Roig-Bataller, A.; Mata-Roig, M. A Standardised Approach to the Biomechanical Evaluation of Tracheal Grafts. *Biomolecules* **2021**, *11*, 1461.
(22) Ouyang, L.; Yao, R.; Zhao, Y.; Sun, W. Effect of Bioink Properties on Printability and Cell Viability for 3D Bioplotting of Embryonic Stem Cells. *Biofabrication* **2016**, *8*, No. 035020.
(23) Park, J.-H.; Yoon, J.-K.; Lee, J. B.; Shin, Y. M.; Lee, K.-W.; Bae, S.-W.; Lee, J.; Yu, J.; Jung, C.-R.; Youn, Y.-N.; Kim, H.-Y.; Kim, D.-H. Experimental Tracheal Replacement Using 3-Dimensional Bioprinted Artificial Trachea with Autologous Epithelial Cells and Chondrocytes. *Sci. Rep.* **2019**, *9*, 2103.
(24) Jariwala, S. H.; Lewis, G. S.; Bushman, Z. J.; Adair, J. H.; Donahue, H. J. 3D Printing of Personalized Artificial Bone Scaffolds. *3D Print. Addit. Manuf.* **2015**, *2*, 56−64.
(25) Koons, G. L.; Mikos, A. G. Progress in Three-Dimensional Printing with Growth Factors. *J. Controlled Release* **2019**, *295*, 50−59.
(26) Jeong, S. I.; Kim, B.-S.; Lee, Y. M.; Ihn, K. J.; Kim, S. H.; Kim, Y. H. Morphology of Elastic Poly(l-Lactide-Co-ε-Caprolactone) Copolymers and in Vitro and in Vivo Degradation Behavior of Their Scaffolds. *Biomacromolecules* **2004**, *5*, 1303−1309.
(27) Tsukada, H.; Gangadharan, S.; Garland, R.; Herth, F.; DeCamp, M.; Ernst, A. Tracheal Replacement with a Bioabsorbable Scaffold in Sheep. *Ann. Thorac. Surg.* **2010**, *90*, 1793−1797.
(28) Agarwal, R.; Blum, K. M.; Musgrave, A.; Onwuka, E. A.; Yi, T.; Reinhardt, J. W.; A Best, C.; Breuer, C. K. Degradation and in Vivo Evaluation of Polycaprolactone, Poly(ε-Caprolactone-Co-L-Lactide), and Poly-L-Lactic Acid as Scaffold Sealant Polymers for Murine Tissue-Engineered Vascular Grafts. *Regener. Med.* **2019**, *14*, 627−637.
(29) Habib, A.; Sathish, V.; Mallik, S.; Khoda, B. 3D Printability of Alginate-Carboxymethyl Cellulose Hydrogel. *Materials* **2018**, *11*, 454.

https://doi.org/10.1021/acsomega.1c06679
ACS Omega 2022, 7, 7002−7011